Characterizing wave-induced mixing energy in OHMSETT wave basin for dispersant effectiveness testing

David W. Wang and Hemantha W. Wijesekera

Oceanography Division, Naval Research Laboratory, Code 7332,

Stennis Space Center, MS 39529

Acknowledgements

This study was funded by the Bureau of Safety and Environmental Enforcement (BSEE), U.S. Department of the Interior, Washington D.C. under Contract E14PG00059, Project 1059.

Disclaimer

This final report has been reviewed by BSEE and approved for publication. Approval does not signify that the contents necessarily reflect the views or policies of BSEE, nor does mention of trade names or commercial products constitute endorsement or recommendation for use.

Table of Contents

Executive Summary

The goal of this study is to quantify and characterize the mixing energy under breaking wave actions in the Ohmsett facility. Mixing energy associated with surface wave breaking in the wave tank was evaluated by estimating turbulent kinetic energy (TKE) directly from measurements of microscale velocity shear. A total of 38 test runs were carried out to measure turbulent mixing levels for two types of wave conditions, namely (1) long-duration wave action for the standard dispersant effectiveness tests and (2) short-duration wave actions prior to the presence of reflected waves from the tank boundary. The wave conditions for the dispersant effectiveness testing were based on wave maker setting of frequency 33.3 cycles per minute and stroke distance of 15.2 cm. Wave conditions for the rest of the test runs were based on wave maker settings of 35 and 40 cycles per minute and 15.2 and 20.3 cm. Surface wave characteristics, TKE dissipation rates, background currents, and temperature and salinity in the tank were collected from multiple sensing packages mounted on the tank bridge-platform while moving at a speed of 0.53 m/s. The major findings of this study are:

- The monochromatic waves generated by the wave maker modulated rapidly into wave groups as they propagated downstream. The period of the modulated wave group was 4 to 10 times larger than the period of the initial monochromatic wave produced by the wave maker. Largest near-surface TKE dissipation rates were found at or near the center of the modulated wave group. Our observations indicate that wave breaking occurs when the wave steepness reaches the critical geometric limit during the modulation process. During wave breaking events, the near-surface TKE dissipation rate reached to about of the order of 10^{-2} (hereafter O( )) W/kg which is

two to three orders of magnitude larger than before and after the wave breaking. The strongest dissipation was observed within the near-surface layer of thickness equivalent to a significant wave height of about ~ 0.4 m.

- Vertical profiles of TKE dissipation rate, $< \varepsilon >$, were constructed for long- and short-duration wave actions. For wave breaking under short-duration wave actions without the effects from wave reflections, $< \varepsilon >$ decreased from O(10^{-3}) W/kg at 0.15 m to O(10^{-5}) W/kg at 0.4 m below the water level. However, $< \varepsilon >$ decayed rapidly with depth under long-duration wave actions (i.e., dispersant effectiveness test), where $< \varepsilon >$ dropped from O(10^{-3})W/kg at 0.15 m to O(10^{-6})W/kg at 0.4 m. The depth dependence of $< \varepsilon >$ can be approximated by the power law, $< \varepsilon > \propto z^{-n}$, where *z* is the depth measured from the water surface, $n = 5$ for the long-duration dispersant effectiveness test, and $n = 3$ for the short-duration test without impact from reflected waves. At depths deeper than 0.4 m below the water level, the TKE dissipation rate of long-duration wave actions was about 3×10^{-6} W/kg, which was one order of magnitude smaller than that of short-duration wave actions.
- The enhancement of the TKE dissipation rate by wave breaking near or at the center of modulated-wave group is consistent with open ocean observations. The magnitude and vertical profile of the TKE dissipation rate under short-duration wave actions are comparable with open ocean observations.

Background

Approximately 3 million gallons of oil are spilled into the waters of the United States every year (NRC 2005). The primary response methods consist of the deployment of mechanical on-water containment and recovery systems. However, mechanical recovery systems often become insufficient when the environmental conditions at the spill are outside the effective operation ranges of the equipment. There is a need to use on-water chemical dispersants to change the inherent chemical and physical properties of oil to enable it to mix with water more easily. The purpose of dispersant is to break up the oil slick spill into numerous small droplets which become rapidly diluted into the water column and subsequently degraded by naturally occurring micro-organisms (NRC 2005). The use of dispersant enhances the amount of oil mixing into the water column. This can greatly reduce the potential contamination effect of surface slicks to habitats and bird, marine mammals and other organisms that live on or near the water surface or shorelines. However, by enhancing the mixing of oil into the water column, dispersant also increase the potential exposure of the water-column to the spill oil. The application of dispersant represents a critical decision making for reducing the risk to organisms at the water surface and near the shoreline while increasing the potential harm to organisms in the water column and at the sea floor. The use of dispersants must be considered carefully, to take into account the pros and cons of using them under various sea-state and weather conditions.

Before any dispersant is approved for application to any spill in US waters, both the toxicity and effectiveness of the chemical dispersants must be evaluated. The effectiveness of chemical dispersants are often evaluated in laboratory standardized bench-scale tests (Kaku et al., 2005), such as the Swirling Flask Test (SFT) and Baffled Flask Test (BFT). The mixing process generated in the laboratory flask tests cannot account for the transport and dilution

effects in the water column caused by turbulence induced by the action of surface waves as observed in the open ocean (Venosa et al., 2005; Boufadel et al., 2008). The methods of generating turbulence motions by shaking of laboratory flasks, by breaking surface waves, or by shear-driven near-surface motions are not identical, and therefore the mixing energy in a laboratory set up and in an oceanic environment require better quantification. Furthermore, the efficiency of mixing in both cases would not be similar. In support of an operational validation of the dispersant for oil dispersion effectiveness, a full-scale field evaluation test under various wave conditions is desirable and necessary. However, such a test is logistically difficult and expensive. The applicability of evaluation results are hampered by limited and uncontrolled wave conditions. The large outdoor Ohmsett wave tank facility (Figure 1) is designed and equipped to simulate realistic sea conditions by producing regular waves (up to 1 m height) and random waves that can't be generated in smaller tanks (Li et al., 2008; Wickley-Olsen et al., 2008). The evaluation of dispersant effectiveness can be carried out under controlled and reproducible wave conditions, and is cost effective and operationally feasible. The evaluation of dispersant effectiveness has been carried out in the past using the Ohmsett facility (S. L. Ross, 2005; Mullin & Trudel, 2006).

The mixing energy in the water column resulting from small-scale velocity-shear plays a key role in the breakup of an oil slick into tiny droplets and in dispersion of the spilled oil into the water column in the presence of a chemical dispersant (Venosa et al., 2006; Li et al., 2008). The magnitude of turbulent kinetic energy (TKE) near the surface is the key factor determining the effectiveness of the oil dispersant. Therefore, understanding how TKE dissipation rates of mechanically-generated surface waves relate to various wave conditions is necessary for correlating the wave tank measurements with oceanic observations (Belore et al., 2005).

The turbulent kinetic energy is dissipated by viscous friction. The resulting energy dissipation rate, ε for homogeneous isotropic turbulence is expressed as (Tennekes & Lumley, 1972)

$$\varepsilon = 7.5\nu\left\langle\left(\frac{\partial u}{\partial x}\right)^2\right\rangle, \quad (1)$$

where $\left\langle(\partial u/\partial x)^2\right\rangle$ is the variance of the velocity shear in 1/s; ν is the kinematic molecular viscosity in m^2/s; ε is in W/kg, and the angle brackets denote either time or space average. Thus, ε from turbulent velocity shear is directly linked to the intensity of the mixing energy (NRC 2005). When the Reynolds number is sufficiently large, there exists an inertial subrange where production and dissipation scales are separable. The velocity shear variance can be estimated by resolving the spatial gradient of turbulent velocity fluctuations at scales ranging from O(mm) to O(m). Therefore the dissipation method (or shear spectral method) provides a direct estimate of the TKE dissipation rate.

The goal of this project is to provide a scientifically validated method to determine mixing energy based on direct measurements of the TKE dissipation rate in the wave tank under wave conditions comparable to the oceanic environment. This report describes methodology and findings of direct measurements of TKE dissipation rates in the Ohmsett wave tank. Section 2 provides a description of the experiment facility and instrumentation setup. Section 3 discusses measurement procedure and data processing. Results and discussion are presented in Section 4. Finally, a short summary and recommendations are given in Section 5.

Experiment facility and Instrumentation

We conducted two experiments at the Ohmsett tank facility during January 12-17, and during September 21-25, 2015. Each experiment consisted of multiple test runs covering a wide range of wave actions with varying frequencies and amplitudes produced by the wave maker (Tables 1 and 2). The experiment conducted in January 2015 (Table 1) was a proof-of-concept for measuring microscale velocity shear and quantifying platform noise levels from sensors mounted on the bridge platform (Figure 1). In the following, we describe experiment setups, measurements, and results, while focusing on the experiment conducted in September 2015 (Table 2).

Wave tank and Instrument platform

The outdoor tank at Ohmsett is 203 m long, 20 m wide, and 3.5 m deep (Figure 1a). The tank is equipped with a bottom-hinged flap-type wave maker with an adjustable paddle stroke-frequency and distance (Asher, 2005; Guarino et al., 2010; Brown & Guarino, 2010). The wave maker is located at the south end of the tank, and a wave-damping beach system is installed at the north end to reduce wave reflection of incoming waves. During our experiments, the beach was raised from the tank floor to the water line to dampen incident wave energy. Details of the wave damping system are given in Guarino et al. (2010). The Ohmsett tank is equipped with three movable bridges with tow speeds up to 3.2 m/s.

The microstructure measurements were made from sensors mounted on an instrumentation-platform (also referred as the NRL platform), which was constructed by combining a cylindrical pole (hereafter “pole”) attached to a 2.3 m long H-beam. The NRL platform was connected to the main tank-bridge to make underway measurements from the movable bridge. In this set up, only the H-beam was attached rigidly to the bridge (Figure 1b).

The pole was mounted on the beam in such a way that the pole could be moved vertically (up and down) along the beam to position the microstructure-sensors at different depths. Three microstructure sensing packages (MicroRider-1000, hereafter “MR”) and one acoustic Doppler velocimeter (ADV) were mounted on the pole (Figures 1b and c). A Conductivity-Temperature-Depth (CTD) package and another ADV were attached at fixed locations on the H-beam. An upward looking acoustic Doppler current profiler (ADCP) was mounted on a horizontal extension beam attached to the bottom of the H-beam (Figures 1c and d). The flow field around the instrument-platform can be distorted as waves pass the NRL-platform. Therefore the microstructure sensing packages were mounted on the pole so that the turbulent sensors, such as shear probes and fast thermistors were placed about 0.8 m from the center of the H-beam to avoid the distorted flow field (Figure 1c). The ADV was about 0.4 m from the center of the beam. Note that all the sensing elements were directed toward the wave maker.

Apart from measurements inside the tank, background wind speed, wind direction, and air temperature were also recorded from the weather station next to the tank at 8 m above the ground. Environmental conditions and wave maker settings for the two experiments are given in Tables 1 and 2, respectively.

Turbulent shear probe

The turbulence shear probe is part of a self-contained turbulence microstructure sensing package (MicroRider-1000) developed by Rockland Scientific Inc. (e.g., Goodman et al. 2006; Wolk et al. 2009). It is about 10 cm in diameter, 1 m long, and weighs 5.5 kg in air. The nose cone of the instrument (Figure 3) holds the following sensors: two shear probes (SPM-38), two fast-response thermistors (FP07) and high resolution pressure, acceleration and tilt sensors. The instrument is powered by 9 – 18 VDC and data are recorded internally on a memory card.

Sampling frequencies for individual channels can be between 8 Hz and 4096 Hz. Apart from TKE dissipation rates, the MicroRider-1000 is capable of measuring turbulent temperature variance (TTV) dissipation rate. Dissipation rate of TTV is also a mixing energy estimator when stratification is important. The sampling rate of shear probes and fast thermistors is 512 Hz, and the rest of sensors sample at 64 Hz. For the January experiment, only one MR was deployed. For the September experiment, we mounted three MRs at depth intervals of about 0.23 and 0.25 m (Figures 1 and 2). As mentioned above, the three MRs were mounted on the movable pole on the NRL instrument platform that was adjusted vertically to obtain dissipation estimates between 0.16 m and 0.75 m depths (Figure 2).

Acoustic Doppler velocimeters (ADV)

Two acoustic Doppler velocimeters (ADV), owned by Ohmsett, were also used to measure the turbulence velocities under wave actions. The ADV samples the flow field in three perpendicular directions (along tank, cross tank, and vertical) at a rate of 32 Hz. The accuracy of the measurement is about 1 mm/s. One ADV was placed 0.25 m below the three MRs on the movable pole and a second ADV was placed on the beam at depth 1.5 m below the water surface.

Acoustic Doppler current profiler (ADCP)

The ADCP mounted on the bottom of the NRL platform was a 1200-kHz broadband Workhorse Sentinels (RD Instruments). Furthermore, two 600-kHz ADCPs were placed on the bottom of the tank floor (35m and 163 m, respectively, to the wave maker) (Figure 1). The ADCPs recorded profiles of currents and bubble echo intensity during both experiments.

Measurement procedure and Data processing

Measurement procedure

We conducted TKE dissipation measurements for both short- and long-duration wave actions. Tests under short-duration wave actions focused on TKE dissipation measurements prior to the presence of reflected waves from the tank boundary. Tests under long-duration wave actions represented the standard dispersant effectiveness testing (S.L. Ross, 2001).

During short-duration testing, the bridge and instrument-platform were first positioned at a distance of 170 m from the wave maker before starting the wave maker. Once waves were generated, the bridge-instrument platform moved toward the wave maker from its initial position to a location 35 m from the wave maker at a steady towing speed of 0.53 m/s, while encountering wave breaking events and collecting concurrent measurements of microscale velocity shear, currents, and temperature and salinity in the tank. Depending on the wave periods generated by different paddle-frequency settings (Table 2), the waves reflected from the beach end reached the moving bridge and instrument platform within 240 – 290 sec after the start of wave actions.

The protocol of the standard dispersant effectiveness tests at Ohmsett requires a 5-min wave generation for the development of wave conditions prior to the release of oil and dispersant into the tank. The duration of the dispersant effectiveness test can last 30 min or longer (Fingas & Decola, 2006; S.L. Ross, 2001). Strong interactions among incoming and reflected waves were observed during the long-duration wave actions. TKE production and dissipation rates under these long-duration wave actions were affected by reflected waves.

For a given test run, microscale velocity shears were measured at three different depths with vertical spacing of about 0.23 and 0.25 m (Figure 1c and Table 2). Each test run lasted about 250 sec. We repeated this measurement procedure to construct vertical profiles of TKE

dissipation rates by adjusting the vertical position of the pole at increments of 2 cm to 5 cm to construct vertical profile of TKE dissipation rate between 0.16 m and 0.75 m below the water level. The wave maker settings for wave actions of monochromatic as well as random waves based on the Pierson–Moskowitz (PM) spectra are given in Tables 1 and 2.

TKE dissipation from shear probe measurements

For homogeneous isotropic turbulence, the TKE dissipation rate is computed from the variance of the turbulent velocity gradients (1). In practice, the velocity shear variance, $<(\partial u/\partial x)^2>$, is estimated directly by integrating the shear spectrum from a specified wavenumber band ranging from a low-wavenumber representing inertial subrange motions to the dissipation wavenumber (or the Kolmogorov wavenumber, $(\varepsilon/\nu^3)^{1/4}$). However, when turbulent motions are highly energetic, such as during surface wave-breaking events, the shear probes used in microstructure sensing packages do not fully resolve the shear spectrum at higher wavenumbers, thus underestimating the TKE dissipation rate. When the turbulent dissipation is weak, and the background noise is large or comparable with the velocity shear signal, shear probes observations are contaminated by the background noise (such as vibrations resulting from the measuring platform). Therefore, the area under the measured velocity shear spectra represents only part of the total variance of shear. To estimate the dissipation rate, the measured shear spectra are fit to the Nesmith universal spectrum (Oakey, 1982; Wolk et al., 2009) or the theoretical spectral shape in the inertial-subrange

$$\phi(k) = A_1 \alpha (2\pi)^{4/3} \varepsilon^{2/3} k^{1/3}, \qquad (2)$$

where A_1=24/55 for the transverse spectrum, and α=1.5 is the universal constant. Note that the wavenumber *k* is in cycles per meter (hereafter cpm). The dissipation rate can be estimated by fitting the theoretical form of $\phi(k)$ (2) to the observed shear spectrum, $\phi_M(k)$, in the inertial

subrange wavenumber band from k_a to k_b. By combining (2) and the observed transverse wavenumber spectrum, $\phi_M(k)$, we determined the TKE dissipation rate as (e.g.,Tennekes & Lumley, 1972; Bluteau et al., 2016):

$$\varepsilon = [(4/3)E/(A_1\alpha(2\pi)^{4/3}(k_b^{4/3} - k_a^{4/3})]^{3/2}, \qquad (3)$$

where $E = \int_{k_a}^{k_b} \phi_M(k)\, dk$.

During the experiments, the two shear probes in each MR were mounted orthogonal to each other to measure the cross-stream and vertical velocities gradients while the sensor platform was moving along the tank or the along-stream direction. We computed transverse spectra of velocity shear for the two orthogonal components (cross-stream and vertical), and then averaged both together to construct a representative spectrum for a given data segment, $\phi_M(k)$, where k is the wavenumber in the direction of the mean flow (i.e., along the tank-axis). The measurements from the moving platform enable the conversion of the velocity-shear frequency spectrum into a wavenumber spectrum using Taylor's frozen turbulence hypothesis. For a sampling rate of 512 Hz and a platform speed of 0.53 m/s, velocity fluctuations can be resolved at 1 mm spatial scales. Velocity-shear frequency spectra, $\phi_M(f)$, were calculated for 1-sec segments of velocity-shear measurements. The frequency spectra $\phi_M(f)$ were converted to the wavenumber spectrum, where $\phi_M(k) = U_B\phi_M(f)$, $k=f/U_B$, U_B is the towing speed of the bridge in m/s, and f is the frequency in Hz. Examples of velocity shear spectra for 1-sec data segments from Test 15 (Table 2) for three different dissipation levels are illustrated in Figure 4 along with the Nasmyth empirical spectrum. The TKE dissipation rate (3) was evaluated first by averaging spectral estimates from two shear probes, and then by integrating the averaged shear spectrum between

k_a=10 cpm and k_b=35 cpm. Estimated TKE dissipation rates based on (3) for the spectra shown in Figure 4 are 2.99×10^{-6} W/kg, 1.37×10^{-4} W/kg, and 7.35×10^{-2} W/kg, respectively.

TKE dissipation from ADV measurements

We collected three-dimensional turbulent velocity fluctuations in the along-stream (along-tank), cross-stream (cross-tank), and vertical directions from the ADVs mounted on the platform. The sampling rate of 32 Hz was sufficient to resolve the inertial-subrange velocity fluctuations at a bridge speed of 0.53 m/s. As discussed above, the inertial-subrange velocity spectral level can be used to evaluate the TKE dissipation rate by fitting a theoretical turbulent longitudinal velocity spectrum,

$$\phi_u(k) = A_2 \alpha (2\pi)^{-2/3} \varepsilon^{2/3} k^{-5/3} \ , \qquad (4)$$

where A_2=18/55. The velocity frequency spectrum, $\phi_{uM}(f)$ was computed for each 10-second segment of ADV data, and then the wavenumber spectrum, $\phi_{uM}(k)$ was constructed by following Taylor's frozen hypothesis, where $\phi_{uM}(k) = U_B \phi_{uM}(f)$. Examples of $\phi_{uM}(k)$ from the two ADVs at 0.9 m and 1.5 m depths during Test 15 are shown in Figures 5a and b, respectively (Table 4). The spectral peaks in Figure 5a represents the wave orbital velocity motions of the monochromatic waves generated by the wave maker with a frequency setting of 35 cycles per minute. Note that peak wavenumbers (Figure 5) of the velocity spectra from the ADVs on the NRL platform were a slightly higher than those corresponding to the paddle frequency due to the Doppler shift by the platform's moving speed U_B. At higher wavenumbers, a -5/3 spectral slope can be clearly identified despite the presence of a spectral peak at wavenumber 7.5 cpm, which could be caused by vibration of the bridge during towing. By fitting the velocity spectra, $\phi_{uM}(k)$, to the spectral model (4) between k=3.5 cpm and 5.5 cpm, TKE dissipation rates were estimated.

Resulting dissipation rates for the spectra shown Figures 5a and b, are about $2x10^{-4}$ W/kg and $3x10^{-5}$ W/kg, respectively.

Wave parameters

During the experiments, surface wave elevations were obtained from measurements by pressure sensors in the MRs at a sampling rate of 512 Hz and by the downward-looking sonic-altimeters mounted on the bridge platform at a sampling rate of 10 Hz. Surface wave elevations estimated from the altimeters and the pressure sensors were very similar. For a better synchronization with velocity shear measurements from the MRs, we used surface elevations derived from the pressure sensor in MR121 (Figure 1c). Wave actions in the tank were characterized by the significant wave height, $H_S = 4\sigma^{1/2}$, where σ is the variance of wave elevation of a specified time segment. In addition, the local wave amplitude, a, and frequency, f_p, were derived from wave elevations by using the wavelet analysis method (Huang et al., 2007; Wang & Wijesekera, 2017). The local frequency, f_p, was corrected for the Doppler shift by the moving platform. We then computed the local steepness, $\delta = a\omega^2 / g$, where $\omega = 2\pi f_p$ and g is the gravitational constant.

Results and Discussion

During these experiments, TKE dissipation measurements were carried out under wave actions with frequent occurrences of wave breaking. Figure 6a shows a snap shot of whitecap formations from wave breakings. The occurrences of whitecaps were evenly distributed in the along-tank direction but with considerable patchiness. Figure 6b shows a wave breaking event near the instrument-platform. Depth-averaged velocity between 0.4 m and 0.6 m (Figure 7) was obtained from the bottom mounted ADCP placed at 163 m from the wave maker (Figure 1). The

5-min averaged, along- and cross-tank velocities fluctuated with a magnitude of 5 cm/s or less during the experiment. The backscatter echo-intensity from the ADCP increased when the wave maker was running and the background flow was relatively large (Figure 7b). The deepening of high echo-intensity (Figure 7b) suggests stirring and movement of particles in the tank by currents and turbulent motions, and entrainment of bubbles generated by wave breaking. Time series of temperature and salinity were also collected from the CTD mounted near the bottom of the tank (Figure 8). CTD observations showed no changes in salinity during the testing period during September 25-26, but the temperature followed a diurnal cycle with a temperature difference of about 1^{o}C. A small increase in temperature (~0.05^{o}C) was found when the wave maker was active (Figure 7b).

TKE dissipation measurements under short-duration wave actions

Two examples of observations of short-duration wave actions made from the MRs are shown in Figures 9 and 10, representing, respectively, paddle stroke frequency (cycles per minute)/distance (cm) of 35/8 (Test 15, Table 2), and 40/6 (Test 5, Table 2). Both tests produced similar results (Figures 9 and 10). In the following, we discuss results from Test 15 in more detail. The 200-sec short segment of measurements, shown in Figure 9, was not affected by the reflected waves from the beach end of the tank. The MRs first encountered the incoming waves from the wave maker at about 10 sec into the measurements (Figure 9a). Surface wave elevations showed highly modulated wave groups as depicted by the wave amplitude (Figure 9a). The modulated wave groups are caused by the Benjamin-Feir instability mechanism (BFM), which is the interaction between a strong carrier harmonic wave and waves at adjacent side-band frequencies. The BFM leads to modulation of the initially monochromatic wave train, and as a result some waves can become very large at the expense of others and ultimately break

(Benjamin & Feir, 1967; Babanin et al. 2007). Figure 9b illustrates time evolution of wave steepness, δ, and microscale velocity-shear squared Sh^2, which is used as an indicator of the TKE dissipation rate. The velocity shear, *Sh*, was obtained by filtering velocity shear measurements of the MR140 between frequencies of 5.3 Hz and 18.6 Hz and the corresponding wavenumbers are 10 cpm and 35 cpm, respectively, for U_B=0.53 m/s. The time series of TKE dissipation rates were estimated from 1-sec segments of velocity shear data at 0.19m, 0.44m and 0.67m below the water level (Figure 9c).

Both δ and Sh^2 peak near or at the center of the wave group (Figure 9b). Modulation instability increased wave steepness to the geometry limits (Tulin & Waseda, 1999; Babanin et al., 2007; Tian et al., 2012), and eventually led to wave breaking while injecting turbulence into the water column. The periodicity of wave breaking at or near the center of the modulated group is similar to observations from the open ocean described by Donelan et al. (1972) and Gemmrich & Farmer (2004). Near-surface TKE dissipation at 0.19 m below the water surface varied in a periodic manner in most occasions. The TKE dissipation rate varied between 10^{-6} W/kg and 10^{-2} W/kg and the strongest dissipations were found during breaking events. The enhancement of dissipation rate was highly correlated with the increasing wave steepness (Figure 9). However, the relationships among wave breaking, wave steepness, and the resulting TKE dissipation rates at depths deeper than one wave height (0.53 m) are less correlated and dissipation rates remained at O(10^{-6}) to O(10^{-4}) W/kg. Similar results were also observed in TKE measurements for slightly different wave maker settings (Figure 10). .

TKE dissipation measurements under long-duration wave actions

Figure 11 shows a 200-sec of wave and TKE dissipation measurements under wave actions after a 5-minute wave development, representing wave conditions for dispersant

effectiveness test (S.L. Ross, 2001). The wave fields under the long-duration wave actions were affected by reflective wave energy. As a result, time series of surface wave elevations show strong wave modulation and formation of wave groups (Figures. 11a and b). Near-surface TKE dissipation rate at 0.21 m below the surface was strongest at or near the center of wave groups (Figure 11c). Wave breakings inject turbulent energy and increase the instantaneous dissipation rate from 10^{-6} W/kg to 10^{-2} W/kg. Variations in TKE dissipations at deeper depths (0.46 and 0.69 m) are less significant under breaking waves. These results are similar to the measurements under short-duration wave actions (Figures 8 and 9).

Results of TKE dissipation measurements are presented by time-averaging TKE dissipation rate, <ε> over a selected 80-sec segment for each test run. Here the 80-sec segment from the moving bridge at U_B=0.53 m/s covers about a 42-m length of the tank. Averaged TKE dissipation rates under short-duration and long-duration wave actions are tabulated in Table 3 and 4, respectively.

Vertical profiles of TKE dissipation

Vertical profiles of TKE dissipation were constructed by time averaging dissipation estimates at depths from 0.15 m to 0.75 m. Figure 12 shows vertical profiles of TKE dissipation for both experiments. The vertical profiles of TKE dissipation rate for long-duration wave actions, $< \varepsilon_L >$ are from the observations made during the second experiment conducted in September 2015 (Table 5). The vertical profiles of TKE dissipation rate for short-duration wave actions, $< \varepsilon_S >$ were obtained by combining both January and September experiments. At depths less than 0.2 m, the near-surface $< \varepsilon_L >$ is O(10^{-4})W/kg, which is comparable with $< \varepsilon_S >$. However, the vertical structure of $< \varepsilon_L >$ and $< \varepsilon_S >$ are significantly different at depths below 0.3 m. $< \varepsilon_L >$ decreases with depth more rapidly than $< \varepsilon_S >$. At depths below 0.4 m, $< \varepsilon_L >$

became one order of magnitude smaller than $<\varepsilon_S>$. These observations suggest that the injected turbulence generated by breaking waves under long-duration wave actions has less impact on the vertical distribution of TKE dissipation as compared to that of short-duration wave actions. The difference in the depth-dependent vertical structure of TKE dissipation is likely caused by the wave flow fields influenced by strong interactions between incident and reflected waves during long-duration wave actions. Further study is needed.

In general, $<\varepsilon_L>$ and $<\varepsilon_S>$ decrease with depth (Figure 12) following a power law relation and can be approximately represented by

$$<\varepsilon_L>= 3\times10^{-8} z^{-5}, \quad 0.1\,\mathrm{m} \le z \le 0.4\,\mathrm{m}, \text{ and} \tag{5}$$

$$<\varepsilon_S>= 5\times10^{-6} z^{-3}, \quad 0.1\,\mathrm{m} \le z \le 0.5\,\mathrm{m}. \tag{6}$$

At depths below 0.4 m, both $<\varepsilon_L>$ and $<\varepsilon_S>$ do not change significantly with depth. $<\varepsilon_L>$ remains about $3\text{x}10^{-6}$ W/kg, which is one order of magnitude smaller than $<\varepsilon_S>$ that is about $4\text{x}10^{-5}$ W/kg.

Comparison with open ocean observations

Near-surface TKE dissipation rates in the ocean are on the order of 10^{-4} to 10^{-2} W/kg for winds reaching 20 m/s and wave heights exceeding 7 m (Thomson et al. 2016). Similar dissipation rates were also found during moderate wind conditions (e.g., Gemmrich, 2010; Schwendeman et al., 2014; Sutherland & Melville, 2015). Germmrich and Farmer (2004) measured TKE dissipation rates associated with individual breaking events at winds up to 14 m/s. They showed that the background TKE dissipation at 1-m depth prior to the breaking event was about $5\text{x}10^{-6}$ W/kg and that the dissipation at the same depth during breaking was as large as

$8x10^{-3}$ W/kg. Furthermore, they reported that wave breaking occurred near the crest of the largest wave in the wave group. These observations are consistent with the magnitude and pattern of dissipation rate enhancement during wave breakings in our tank experiments, even though the length and time scales of waves in the tank are much smaller than wave conditions in the open ocean. More recently, Callaghan et al. (2016) suggested that space and time averaged TKE dissipation rates in actively breaking waves are largely independent of length and time scales of breaking waves. They postulated that more energetic breaking waves increase air entrainment but not significantly increase the averaged turbulent intensity. Vertical profiles of near-surface TKE dissipation in the open ocean tend to follow the power law, z^{-m}, where m varies from 1 to 2 (e.g. Sutherland & Melville, 2015; Thomson et al., 2016), and is close to the vertical structure of $< \varepsilon_S >$ with wave breaking without the influence of reflected waves (6).

TKE dissipation by ADV measurements

During these experiments, TKE dissipation rate was also computed from velocity measurements by the two ADVs. The ADV on the movable pole measured currents at 0.92 to 0.97 m depths. The second ADV was at a fixed depth of 1.5 m. The results are shown in Table 4. The TKE dissipation rates from the ADVs are in the range of $O(10^{-4})$ to $O(10^{-5})$ W/kg that is relatively higher than those from MRs considering that the ADVs are at deeper depths. We suspect this could be caused by contamination of velocity data at high frequencies due to the vibration from the moving platform as shown in Figure 5. Veron (2009) measured dissipations by an ADV at 0.53 m depth and reported dissipation in the range of $O(10^{-3})$ to $O(10^{-4})$W/kg. Further study is needed for the validity of using ADV measurements for TKE dissipation at Ohmesett.

Conclusions

A total of 38 test runs were carried out to evaluate turbulent mixing levels for two types of wave conditions, namely (1) long-duration wave action for the standard dispersant effectiveness tests, and (2) short-duration wave actions prior to the presence of reflected waves from the tank boundary. The monochromatic waves, generated by the wave maker, modulated rapidly into wave groups as they propagated downstream. Periods of the modulated wave groups were 4 to 10 times the initial periods of the monochromatic waves. Largest near-surface TKE dissipation rates were found at or near the center of the modulated wave groups, where the wave steepness was large. The observations suggest that the modulation instability increased wave steepness to its critical geometric limit, thus initiating wave breaking. During wave breaking events, the near-surface TKE dissipation was on the order of 10^{-2} W/ kg, which was two to three orders of magnitude larger than before and after the wave breaking. The strongest turbulent mixing was limited to a near-surface layer of about 0.4 m (~ equivalent to a significant wave height).

Vertical profiles of TKE dissipation rate were constructed by time-averaging dissipation estimates. The vertical profiles of long-duration wave actions, $< \varepsilon_L >$, and short-duration wave actions, $< \varepsilon_S >$, are comparable at depths less than 0.2 m. However, the vertical structure of $< \varepsilon_L >$ and $< \varepsilon_S >$ were significantly different at deeper depths. $< \varepsilon_L >$ decreased with depth more rapidly than that of $< \varepsilon_S >$. At depths below 0.4 m, $< \varepsilon_L >$ became one order magnitude smaller than $< \varepsilon_S >$. The depth dependence of $< \varepsilon >$ can be approximated by the power law, $< \varepsilon > \propto z^{-n}$, where *z* is the depth from the water surface, $n = 5$ for long-duration dispersant effectiveness tests, and $n = 3$ for short-duration tests without impact from reflected waves.

The enhancement of TKE dissipation by wave breaking occurring near or at the center of wave groups is consistent with the open ocean observations. The magnitude and vertical profile of TKE dissipation rate under breaking waves of short-duration wave actions are comparable with open ocean observations.

Recommendations

1. We find significant differences in the vertical structure of TKE dissipation rate for wave breaking under short-duration monochromatic wave actions and long-duration more complex wave conditions caused by reflected waves. The vertical structure of TKE dissipation rate under short-duration wave actions is closer to results from field observations. We recognize that the dispersant effectiveness test at Ohmsett requires a long-duration of wave actions (30 min or longer, S. L. Ross 2001). Therefore, the impacts of reflective waves on wave breaking, breaking mechanisms, and the resulting energy dissipation under long-duration wave actions should be further examined. The energy-damping setup in the tank partially absorbs the incident wave energy, and the wave conditions under the effect of reflected waves could result in stronger modulations, and more wave breakings. We recommend that vertical profile measurements of TKE dissipation should be conducted at a fixed time interval to characterize the temporal and spatial evolution of TKE dissipation under longer duration wave actions.
2. A redesign of the energy damping beach to reduce impacts of wave reflections during long-duration tests should be considered.

References

Asher, W. (2005). Data report for a wave characterization study at the Ohmsett wave basin. Report to Minerals Management Service.

Babanin, A., Chalikov, D., Young, I., & Savelyev, I. (2007). Predicting the breaking onset of surface water waves. *Geophysical Research Letters*, *34*(7).

Belore, R. C.,Trudel, B. K., & Lee. K., (2005). Correlating wave tank dispersant effectiveness tests with At-Sea trials. in *International Oil Spill Conference*, 1, 65-70, American Petroleum Institute.

Benjamin, T. B., & Feir, J. E. (1967). The disintegration of wave trains on deep water Part 1. Theory. *Journal of Fluid Mechanics*, 27(03), 417-430.

Bluteau, C. E., Jones, N. L., & Ivey, G. N., (2016). Estimating turbulent dissipation from microstructure shear measurements using maximum likelihood spectral fitting over the inertial and viscous subrange. *Journal of Atmospheric and Oceanic Technology*, 33, 4, pp. 713-722.

Boufadel, M. C., Wickley-Olsen, E., King, T., Li, Z., Lee,K., & Venosa. A. D., (2008). Theoretical foundation for predicting dispersion effectiveness due to waves. in *International Oil Spill Conference*, Vol. 2008, No. 1, pp. 509-513. American Petroleum Institute.

Brown, N., & Guarino, A., (2010). The Ohmsett Ocean Energy Test Facility, In proceedings of *the 29th American Towing Tank Conference*, p. 165-170.

Callaghan, A. H., Deane, G. B., & Stokes, M. D. (2016). Laboratory air-entraining breaking waves: Imaging visible foam signatures to estimate energy dissipation. *Geophysical Research Letters* 43, no. 21.

Donelan, M., Longuet-Higgins, M. S. & Turner, J. S., (1972). Periodicity in whitecaps. *Nature*, Vol. 239, pp. 449-451.

Fingas, M. F., & Decola, E. (2006). Oil Spill Dispersant Effectiveness Testing in OHMSETT, February-March 2006. Prince William Sound Regional Citizens' Advisory Council.

Gemmrich, J., (2010). Strong turbulence in the wave crest region. *J. Phys. Oceanogr.*, 40, 583–595

Gemmrich, J., & Farmer, D., (2004). Near-surface turbulence in the presence of breaking waves. *J. Phys. Oceanogr.*, 34, 1067–1086,

Goodman, L., Levine, E. R., & Lueck, R. G., (2006). On measuring the terms of the turbulent kinetic energy budget from an AUV. *Journal of Atmospheric & Oceanic Technology*, 23(7).

Guarino, A., Schmidt, B., Meyer, P., & Delgado, J., (2010). Recent Testing, Training, and Research Conducted at Ohmsett - The National Oil Spill Response Research & Renewable Energy Test Facility. In *proceedings of the 29th American Towing Tank Conference*, p. 147-156.

Huang, Z. C., & Hwung, H. H., (2007). Local properties of wave modulation observed by wavelet analysis. In *the Seventeenth International Offshore and Polar Engineering Conference*. International Society of Offshore and Polar Engineers.

Kaku, V. J., Boufadel, M., & Venosa, A. D., (2005). Evaluation of turbulence parameters in laboratory flasks used for dispersant effectiveness testing. *International Oil Spill Conference Proceedings*, 395- 398

Li, Z., Lee, K., King, T., Boufadel, M. C., & Venosa, A. D., (2008). Assessment of chemical dispersant effectiveness in a wave tank under regular non-breaking and breaking wave conditions. *Marine Pollution Bulletin* 56, 903-912.

Lueck R. G., Wolk, F., & Yamazaki, H., (2002). Oceanic velocity microstructure measurements in the 20th Century. *Journal of Oceanography*. Vol 58, 153-174.

Mullin, J. V., & Trudel, K., (2006). Five years of dispersant testing in the OHMSETT wave tank: controversial problems, limits of response technology, methods and training. Proceedings from Interspill. NRC.

National Research Council (2005).Understanding oil spill dispersants: Efficacy and Effects. National Academies Press. Washington DC.

Oakey, N. S. (1982). Determination of the rate of dissipation of turbulent energy from simultaneous temperature and velocity shear microstructure measurements. *J. Phys. Oceanogr.*, *12*, 256-271.

S.L. Ross Environmental Research Ltd. (2001). Ohmsett dispersant test protocol development, Report to the U.S. Department of the Interior, Minerals Management Service, Herndon, VA.

S.L. Ross Environmental Research Ltd. (2005). Dispersant effectiveness testing: Relating results from Ohmsett to at-sea tests. Report to the U.S. Department of the Interior, Minerals Management Service, Herndon, VA.

Schwendeman, M., Thomson, J., & Gemmrich, J., (2014). Wave breaking dissipation in a young wind sea. *J. Phys. Oceanogr.,* 44, 104–127,

Sutherland, P., & Melville, W. K. (2015). Field measurements of surface and near-surface turbulence in the presence of breaking waves. *J. Phys. Oceanogr.,* 45, 943-965.

Tennekes, H. and J. L. Lumley, (1972). *A first course in turbulence*. MIT press, 1972.

Thomson, J., Schwendeman, M. S., Zippel, S. F., Moghimi, S., Gemmrich, J. , & Rogers, W. E. (2016). Wave-breaking turbulence in the ocean surface layer, *J. Phys. Oceanogr.*, 46, 1857–1870.

Tian, Z., Perlin, M., & Choi, W., (2012). An eddy viscosity model for two-dimensional breaking waves and its validation with laboratory experiments. *Phys. Fluids* 24:036601

Tulin, M. P., & Waseda, T. (1999). Laboratory observations of wave group evolution, including breaking effects. *J. Fluid Mech.* 378:197–232

Venosa, A. D., Kaku, V. J., & Boufadel, M., (2005). Measuring energy dissipation rates in a wave tank. International Oil Spill Conference Proceedings,183-196.

Venosa, A. D, Lee, K., Boufadel, M., Li, Z., Wickley-Olsen, E., & King, T., (2006). Dispersant effectiveness as a function of energy dissipation rate in an experiment wave tank. *International Oil Spill Conference Proceedings*: 777-783.

Veron, F. (2009). Surface turbulence measurements at Ohmsett. Report to US Minerals Management Service. S. L. Ross Environmental Research, Ottawa, ON, Canada.

Veron, F., & W. K. Melville, (1999). Pulse-to-pulse coherent Doppler measurements of waves and turbulence. J. Atmos. and Ocean. Technol., 16, 1580-1597. (1999).

Wang, D. W., & Wijesekera, H. W., (2017). Observations of breaking wave energy dissipation under modulated wave groups (to be submitted).

Wickley-Olsen, E., Boufadel, M. C., King, T., Li, Z., Lee, K., & Venosa, A. D., (2008). Regular and breaking waves in wave tank for dispersion effectiveness testing. In *International Oil Spill Conference*, 1, 499-508. American Petroleum Institute.

Wolk, F., Lueck, R.G., & St. Laurent L., (2009). Turbulence measurements from a glider. *13th Workshop on Physical Processes in Natural Waters*, Palermo, Italy, 1-4 September 2009.

Table 1

Summary of setups and environmental conditions for the first mixing energy experiment conducted in January 2015.

Test #	Time (UTC)	wave maker		U_B	Environmental condition			Remarks
		Fs	Ds		u (m/s)	θu (°)	T_{air} (°F)	
1	**Jan 14** 19:49	0	0	0.53	2.0	47	32	Tank water salinity is 22.5psu and water temperature is 31.1F at 4' depth
2	20:01	20	7.6	0.53	2.8	58	32	No breaking waves
3	20:21	20	7.6	0.53	3.0	97	32	No breaking waves
4	21:38	40	15.2	0.53	2.8	75	32	
5	**Jan 15** 14:33	40	15.2	0	2.9	300	29	No MR data
6	14:58	40	15.2	0.53	2.3	302	30	No MR data
7	15:24	40	15.2	0.13	2.9	306	30	No MR data
8	15:53	40	7.6	0.53	3.1	286	31	No MR data
9	16:16	35	20.3	0.53	3.2	298	32	
10	16:41	40	15.2	0.53	3.3	305	32	
11	18:20	40	15.2	0.13	3.0	279	33	
12	18:49	40	7.6	0.53	3.1	261	35	Weak breaking waves
13	19:10	33.3	15.2	0.53	2.7	277	37	5-min wave buildup before the test.
14	19:34	40	15.2	0.53	4.6	275	36	
15	19:50	35	20.3	0.53	5.2	295	36	
16	20:35	40	15.2	0.53	4.6	282	35	
17	20:35	35	20.3	0.53	3.6	286	35	
18	**Jan 16** 13:34	PM spectrum 16 m/s wind		--	5.0	260	33	Aborted due to wave generator issue
19	13:49	40	15.2	0.53	4.3	261	33	Tank water salinity is 21.7 psu and water temperature is 36 F.
20	14:11	40	15.2	0.53	5.3	263	34	
21	14:14	40	15.2	0.53	6.4	264	36	

Note. Wave maker setting Fs and Ds are, respectively, the paddle frequency (cycles per minute) and stroke distance (cm). U_B is the bridge towing speed (m/s) during the experiment. The weather station next to the tank provides environmental conditions of wind speed u (m/s), wind direction θ_u (°) and air temperature, T_{air}(°F).

Table 2

Summary of setups and environmental conditions for the second mixing energy experiment conducted in September 2015

Test	**Time (UTC)**	**wave maker**		**Environmental conditions**				**Remarks**
#		Fs	Ds	U_B	u	θu	Tair	
1	**Sept 23** 19:24	0	0	0.53	1.4	70	77	Tank water salinity is 34.5 psu and water temperature is 71.6 F at 4' depth
2	19:35	40	15.2	0	2.0	70	77	
3	20:05	40	15.2	0.53	2.7	82	76	
4	20:19	35	20.3	0	2.4	85	76	
5	**Sept 24** 13:25	40	15.2	0.53	2.3	38	72	Tank water salinity is 34.6 psu and water temperature is 70.5 F at 4' depth
6	14:15	35	20.3	0.53	3.3	42	73	
7	14:35	33.3	15.2	0.53	3.1	31	74	5-min wave action before starting the TKE measurements (dispersant test condition)
8	15:09	40	15.2	0.53				Missing data from bridge
9	15:23	35	20.3	0.53	2.6	51	75	
10	15:40	33.3	15.2	0.53	2.7	49	76	5-min wave action
11	16:59	40	15.2	0.53	2.4	83	78	
12	17:14	35	20.3	0.53	2.2	85	77	
13	18:05	33.3	15.2	0.53	2.7	111	79	5-min wave action
14	18:19	40	15.2	0.53	2.6	95	80	
15	18:34	35	20.3	0.53	1.8	75	79	
16	18:54	PM spectrum 8 m/s		0.53	2.7	96	80	
17	19:07	PM spectrum 10.6 m/s		0.53	2.9	93	79	

Note. Wave maker setting Fs and Ds are, respectively, the paddle frequency (cycles per minute) and stroke distance (cm). U_B is the bridge towing speed (m/s) during the experiment. The weather station next to the tank provides environmental conditions of wind speed u (m/s), wind direction θ_u (°) and air temperature, T_{air}(°F).

Table 3

Summary of turbulent mixing measurements of the first mixing energy experiment

Test	**wave maker**		**wave**	**TKE dissipation**	
#	Fs	Ds	Hs m	z m	$<\varepsilon>x10^4$ W/kg
19	40	15.2	0.47	0.15	31.81
10	40	15.2	0.43	0.22	2.41
20	40	15.2	0.43	0.30	1.30
14	40	15.2	0.42	0.38	0.41
16	40	15.2	0.41	0.53	0.55
9	35	20.3	0.58	0.22	5.15
15	35	20.3	0.54	0.38	1.29
17	35	20.3	0.59	0.53	0.31
2	20	7.6	0.18	0.22	0.00072
3	20	7.6	0.16	0.22	0.00041
12	40	7.6	0.25	0.22	0.04
13	33.3	15.2	0.50	0.22	1.34

Note. Hs is the significant wave height. **<ε>** is the ensemble average TKE dissipation over the 80-sec TKE dissipation measurements. z is the MicroRider depth to the water line.

Table 4

Summary of turbulent mixing measurements of the second mixing energy experiment.

Test	**wave maker**			**TKE dissipation rate <ε> MR ID**						**TKE dissipation rate <ε> ADV ID**			
				MR 140		MR121		MR088		ADV 9659		ADV 9677	
#	Fs	Ds	Hs m	z m	<ε> x10^4	z m	<ε> x10^4	z m	<ε> x10^4	z m	<ε> x10^4	z m	<ε> x10^4
3	40	15.2	0.41	0.16	9.10	0.41	1.00	0.64	0.55				
5	40	15.2	0.41	0.16	8.31	0.41	1.16	0.64	0.45				
14	40	15.2	0.31	0.19	0.80	0.44	0.07	0.67	0.02	0.90	0.29	1.50	0.27
8	40	15.2	0.39	0.21	1.91	0.46	0.34	0.69	0.38	0.92	0.71	1.50	0.24
11	40	15.2	0.40	0.26	1.33	0.51	0.43	0.74	0.10	0.97	0.41	1.50	0.15
6	35	20.3	0.58	0.16	25.74	0.41	0.06	0.64	0.03				
15	35	20.3	0.53	0.19	20.02	0.44	0.95	0.67	0.82	0.90	2.63	1.50	0.37
9	35	20.3	0.46	0.21	11.72	0.46	0.95	0.69	0.30	0.92	2.14	1.50	0.68
12	35	20.3	0.48	0.26	4.71	0.51	1.01	0.74	0.35	0.97	2.11	1.50	0.48
7	33.3	15.2	0.49	0.16	4.4	0.41	0.03	0.64	0.03				
10	33.3	15.2	0.41	0.21	2.0	0.46	0.05	0.69	0.02	0.92	0.74	1.50	0.05
13	33.3	15.2	0.47	0.26	0.11	0.51	0.02	0.74	0.02	0.97	3.53	1.50	0.24
16	PM spectra 8 m/s			0.19	0.001	0.44	0.001	0.67	0.005				
17	PM spectra 10.6 m/s			0.19	0.004	0.44	0.002	0.67	0.006				

Note. Hs is the significant wave height. **<ε>** is the ensemble average TKE dissipation of 80-sec measurement segments. z is the MicroRider depth to the water surface.

Table 5

Vertical profile of TKE dissipation rate

Depth	**TKE dissipation rate**	**95% confidence interval <ε>**	
z (m)	<ε> x10^4 W/kg	Upper ε x10^4 W/kg	Lower ε x10^4 W/kg
0.16	4.42	10.60	1.84
0.21	2.03	4.49	0.92
0.26	0.11	0.158	0.072
0.41	0.032	0.044	0.024
0.46	0.045	0.065	0.032
0.51	0.022	0.028	0.018
0.64	0.031	0.042	0.023
0.69	0.024	0.030	0.019
0.74	0.021	0.025	0.017

Note. Ensemble average <ε>, upper and lower limits of 95% confidence interval of 80-sec TKE measurement segments under long-duration wave actions generated according to wave maker setting of paddle stroke frequency of 33.3 cycles per minute and distance of 15.2 cm.

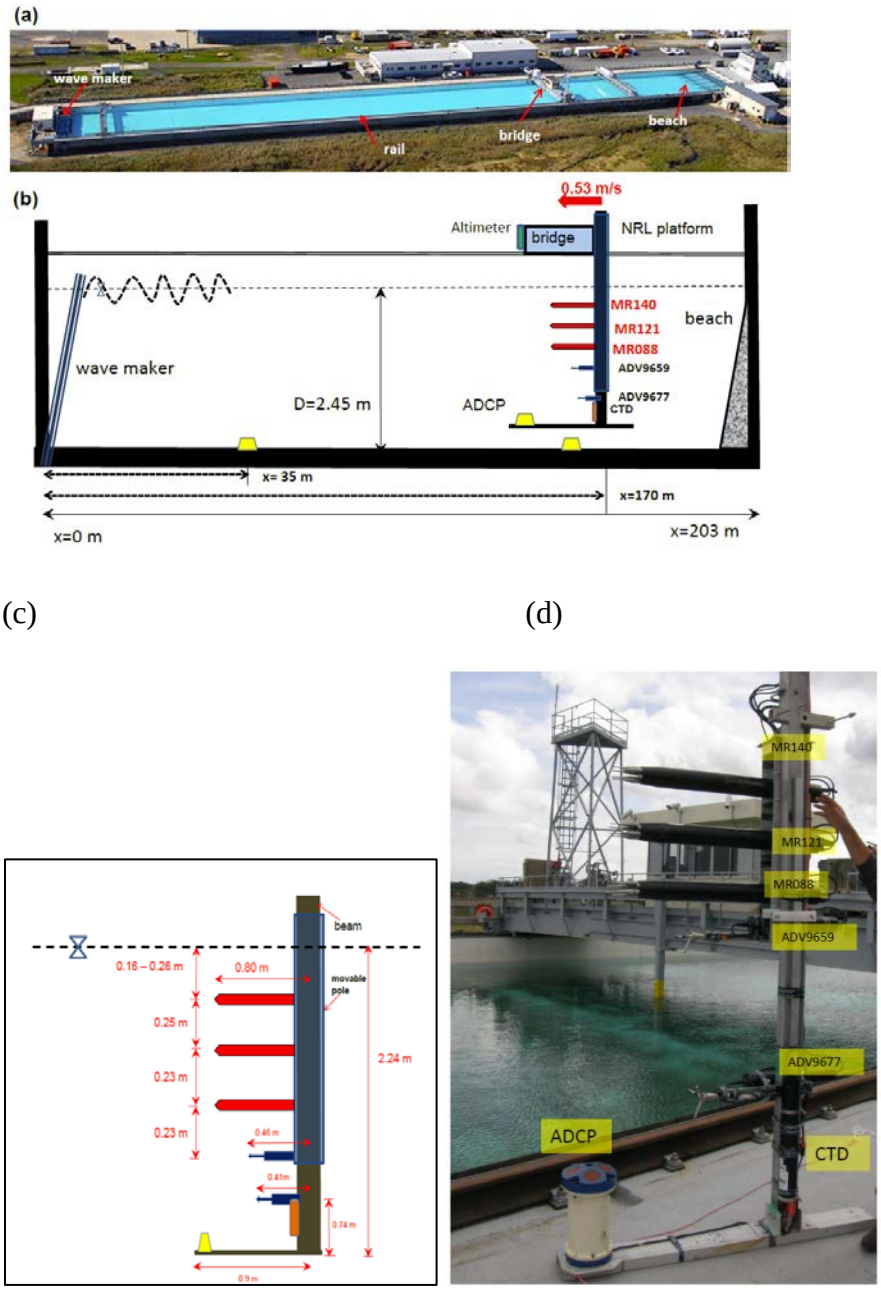

Figure 1. (a) Ohmsett aerial photo, (b) schematic diagram of the wave tank, the NRL instrument platform, and locations of three MRs (red) and two ADVs (blue), three ADCPs (yellow), CTD (brown) and Altimeter (green). (c) Configuration of the instrument platform and sensors, and (d) photo of the platform and mounted sensors before the deployment.

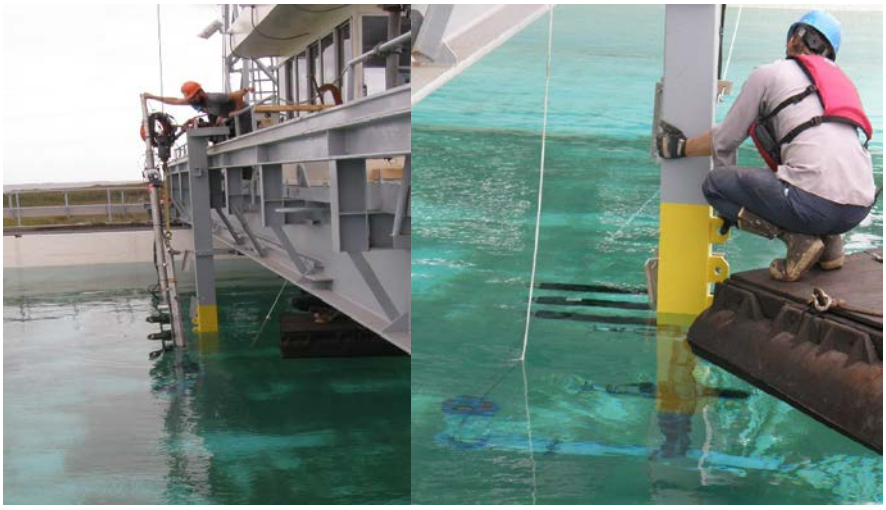

(a) (b)

Figure 2. (a) installation of the instrument platform to the main bridge, and (b) adjustment of platform vertical position during the experiments.

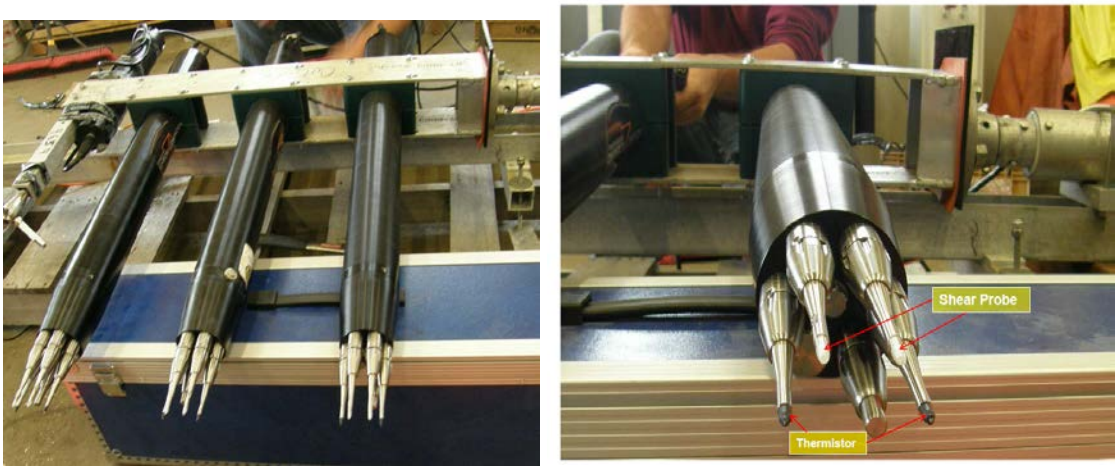

(a) (b)

Figure 3. (a) The three MRs and the mounting bracket of the NRL platform for the second experiment. (b) A close-up look of MR nose cone showing two shear probes and two thermistors.

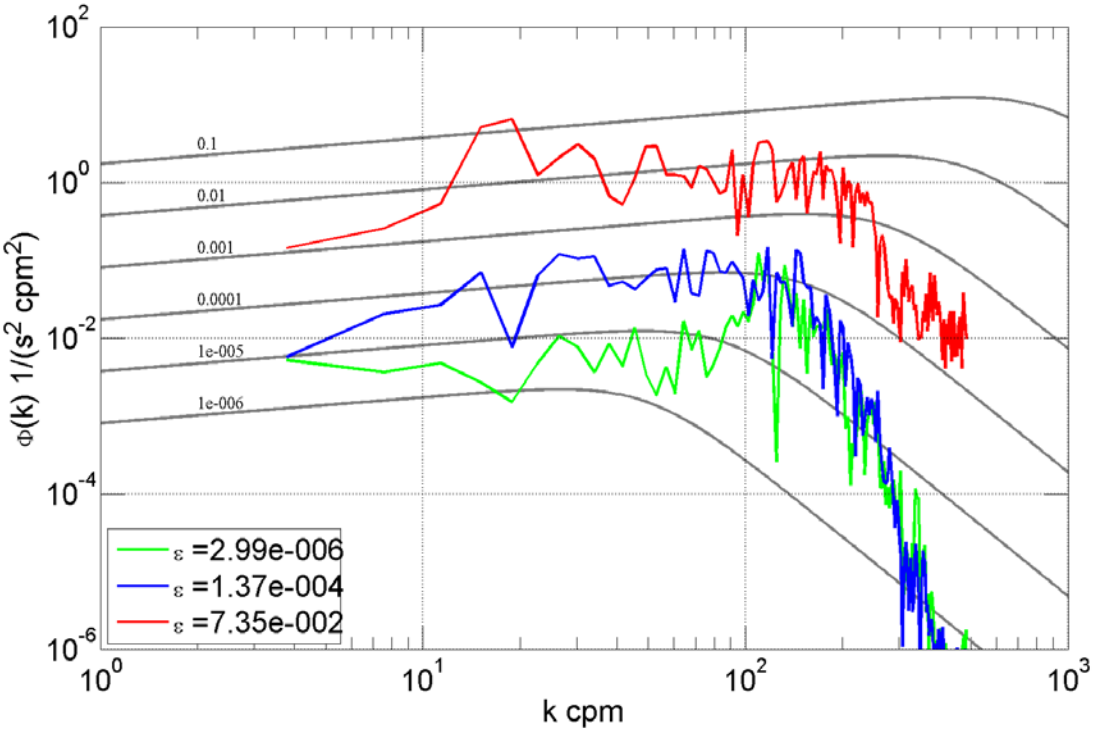

Figure 4. Velocity shear wavenumber spectra for TKE dissipation rate of 2.99×10^{-6}, 1.37×10^{-4} and 7.35×10^{-2} W/kg. The velocity shear data are from the MR140 at 0.19 m depth below water surface during Test 15 (Table 2). The gray curves represent the universal Nysmith spectra for dissipation rates from 10^{-1} to 10^{-6} W/kg.

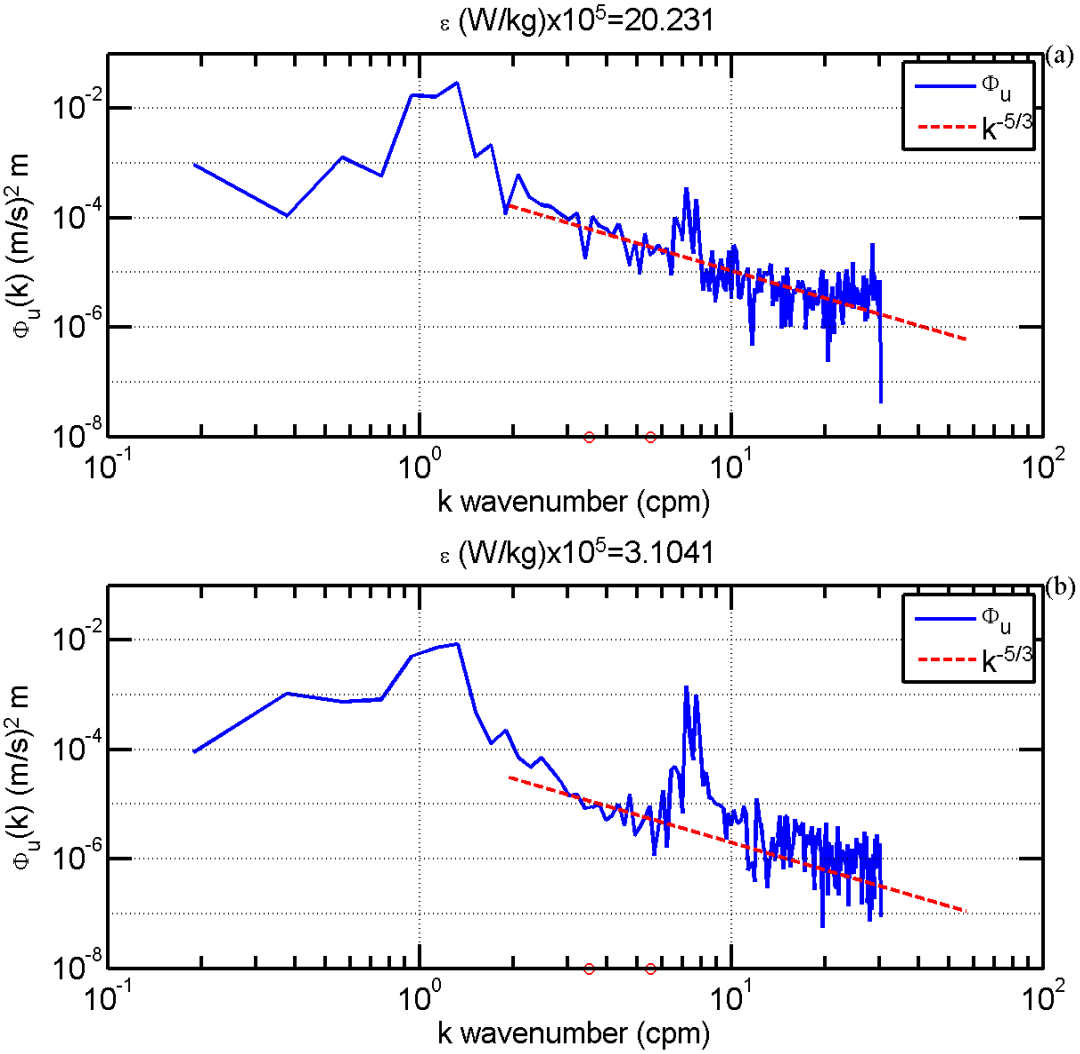

Figure 5. Longitudinal velocity wavenumber spectra from Test 15 by (a) ADV9659 and (b) ADV9677 with TKE dissipation rates $2x10^{-4}$ and $3.1x10^{-5}$ W/kg, respectively. The red dashed lines represent the $k^{-5/3}$ fitting for the inertial subrange based on the spectral energy between 3.5 to 5.5 cpm as indicated by the two red circles, respectively.

(a) (b)

Figure 6. Photos of whitecaps from wave breakings during the experiments. (a) periodic occurrence of whitecaps in along-tank direction (wave is travelling from photo's bottom to top) and (b) whitecap of an individual wave breaking near the NRL platform (wave is traveling away from the platform)

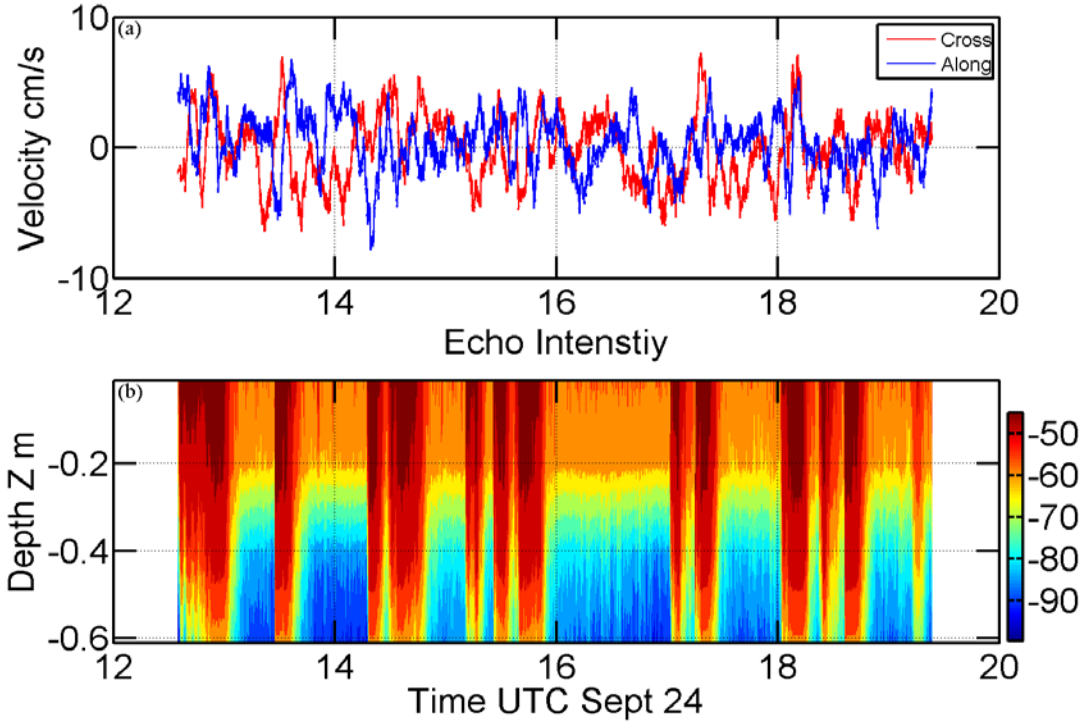

Figure 7. Time series of velocity measurements from the ADCP on the floor (163 m to the wave maker) during the second experiment. (a) 5-min averaged along-tank (blue) and cross-tank (red) velocities between 0.4 to 0.6 m depth (b) vertical profiles of echo intensity.

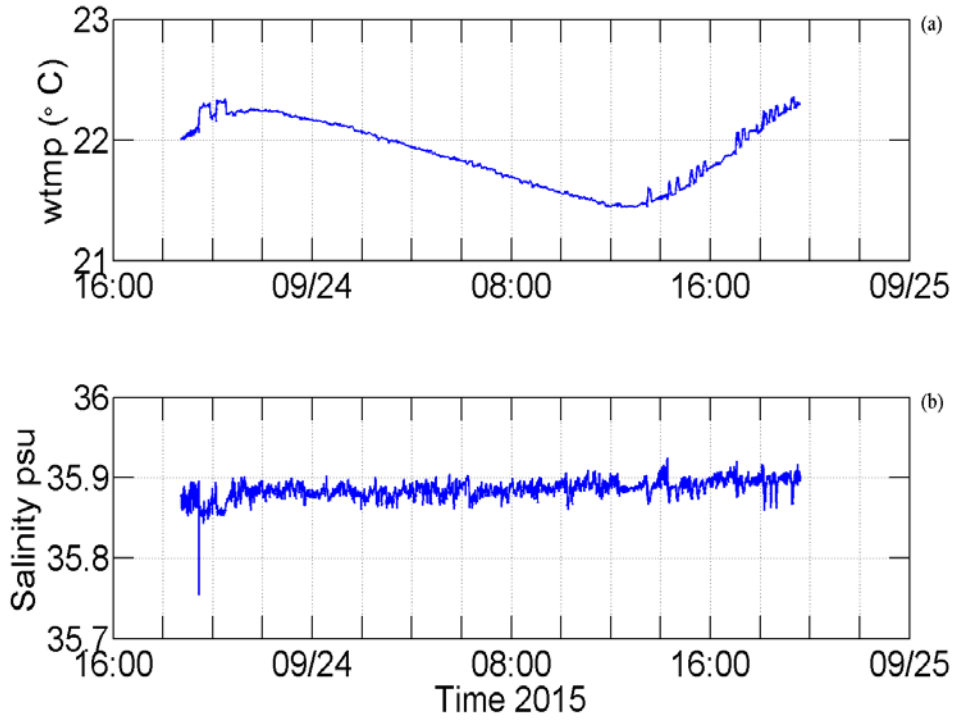

Figure 8. Time series of (a) water temperature and (b) salinity measurements from the CTD during the second experiment.

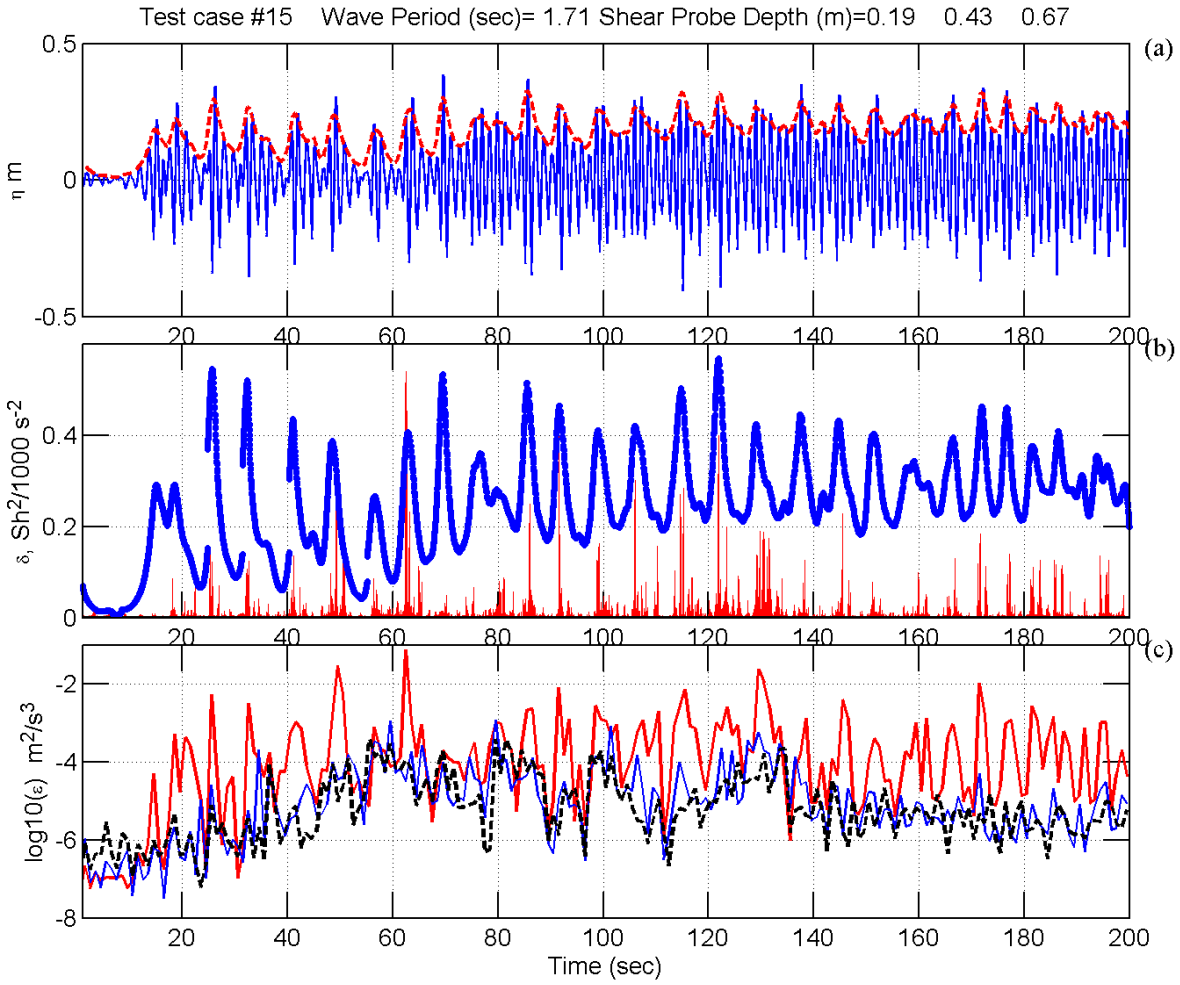

Figure 9. TKE dissipation measurements of Test 15. A 200-sec segment of (a) surface wave elevation(blue) and amplitude of modulated wave group (red dashed line), (b) band-passed velocity-shear squared, $Sh^2/1000$ (red), and wave steepness, δ,(blue) and (c) TKE energy dissipation rate of 1-sec velocity shear measurement segments from the MRs at depths z= 0.19m (red), 0.44m (blue) and 0.67 m (black).

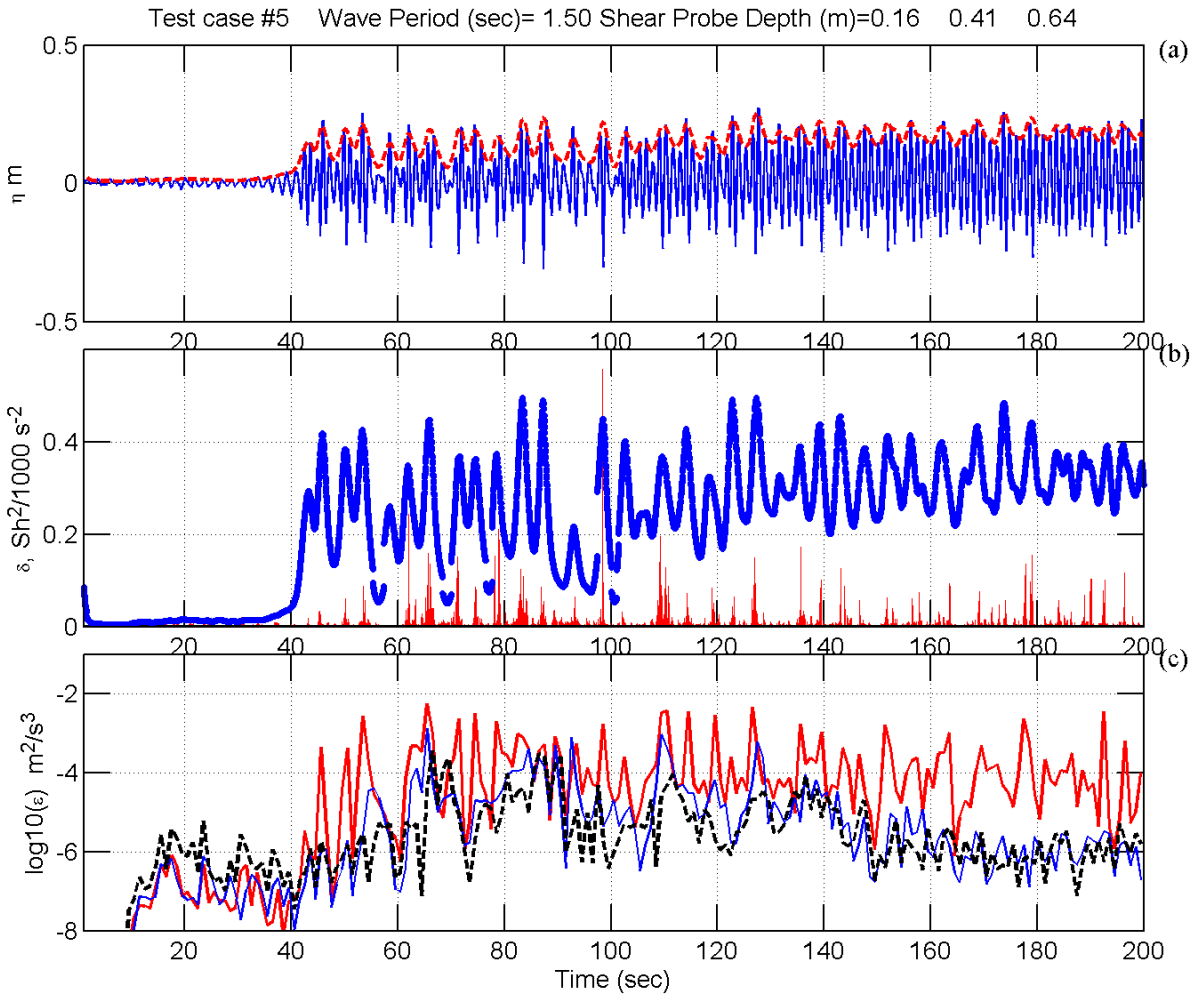

Figure 10. TKE dissipation measurements of Test 5. A 200-sec segment of (a) surface wave elevation(blue) and amplitude of modulated wave group (red), (b) band-passed velocity- shear squared, $Sh^2/1000$, (red) and local wave steepness, δ, (blue) and (c) TKE energy dissipation rate of 1-sec velocity shear measurement segments from the three MRs at depth z= 0.16 (red), 0.41 (blue) and 0.64 m (black), respectively.

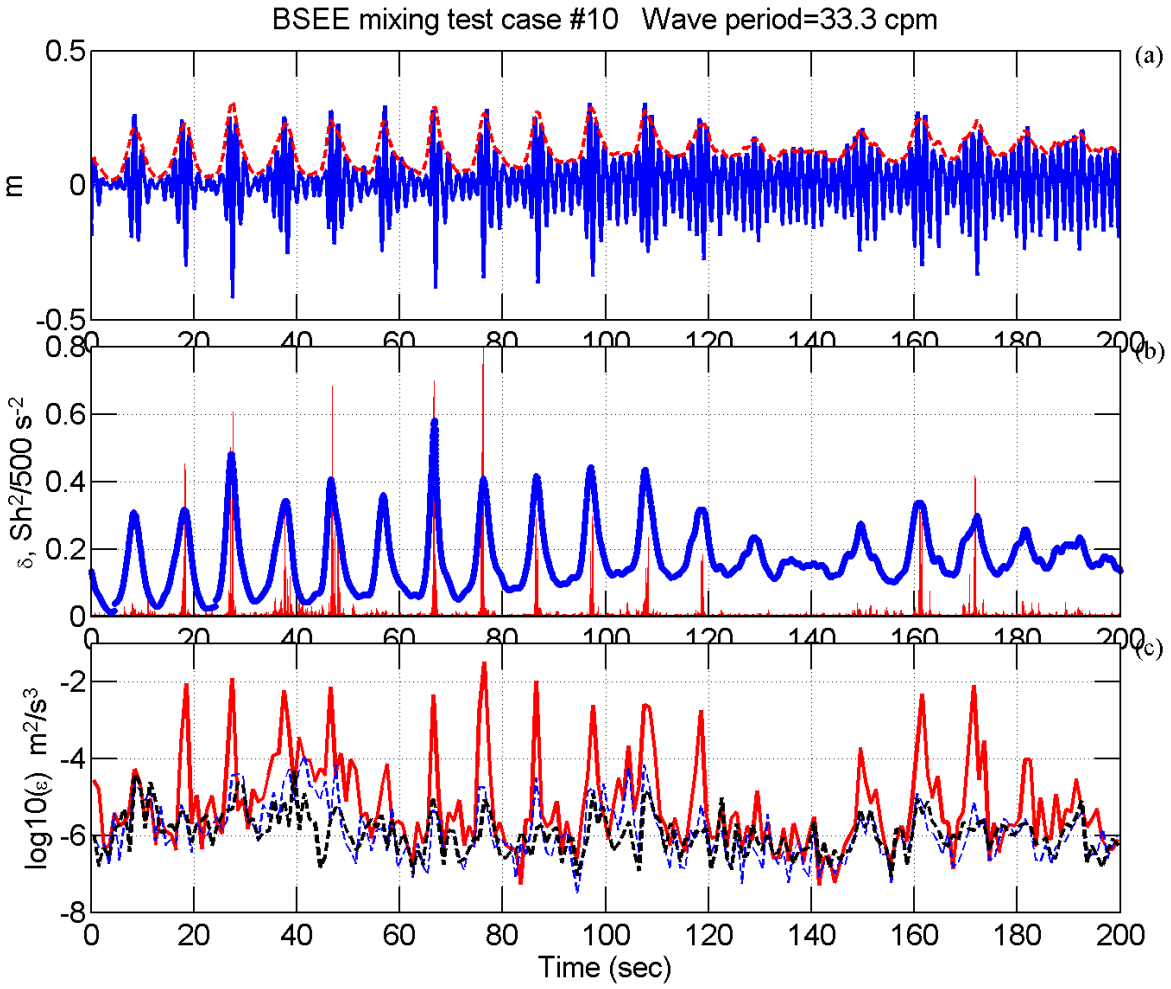

Figure 11. TKE dissipation measurements of Test 10. A 200-sec segment of (a) surface wave elevation(blue) and amplitude of modulated wave group (red), (b) band-passed velocity shear squared, $Sh^2/500$, (red) and local wave steepness, δ, (blue) , and (c) TKE dissipation rate of 1-sec velocity shear measurement segments from MRs at depth z= 0.21 (red), 0.46 (blue) and 0.69 m (black).

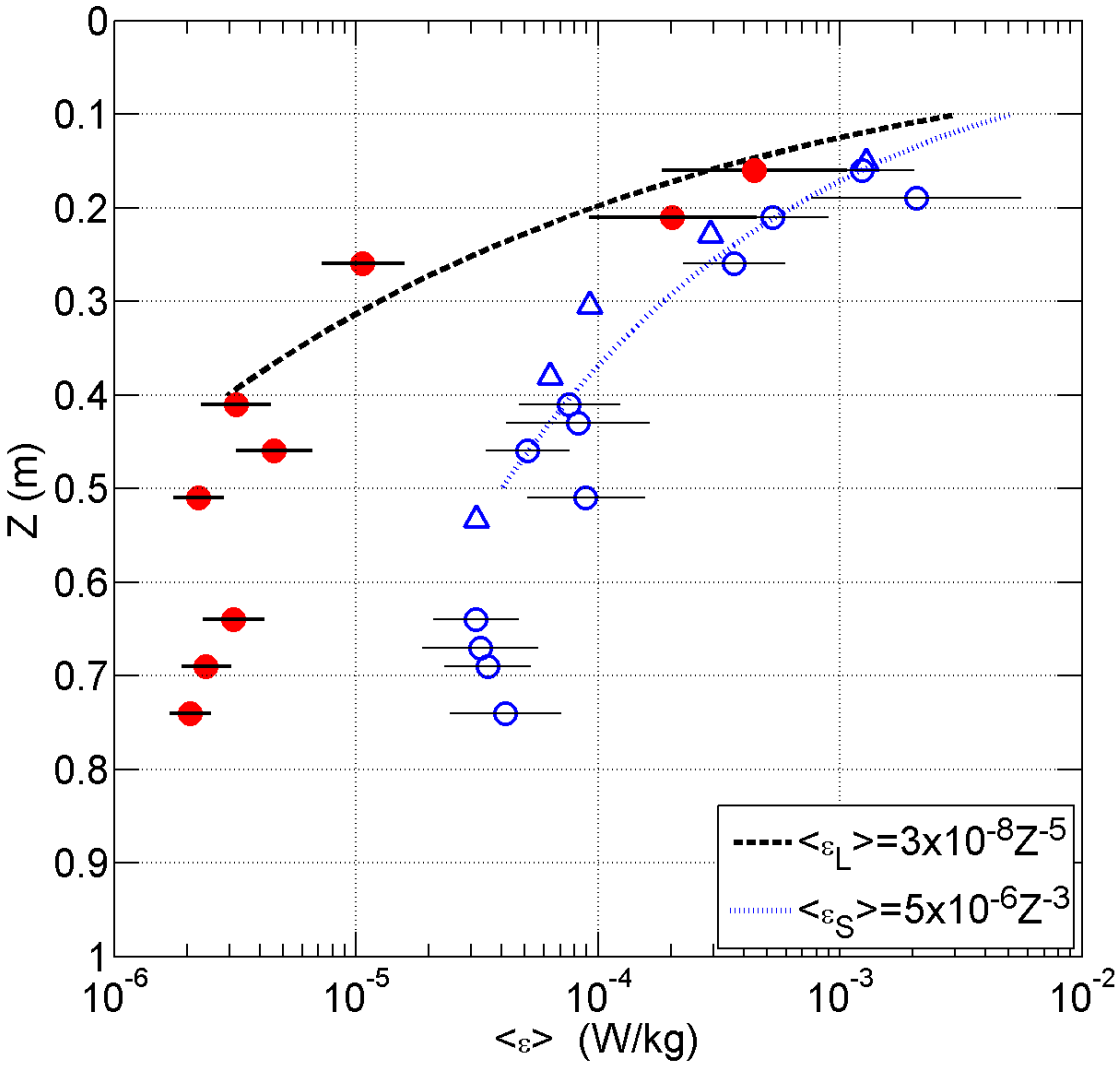

Figure 12. Vertical profile of TKE dissipation under wave actions. $<\varepsilon_L>$ from long-duration wave actions from the second experiment are represented by solid red circles. $<\varepsilon_S>$ from the short-duration wave actions tests of the first and second experiment are represented, respectively, by blue triangles and circles. Horizontal solid lines represent 95% confidence intervals. The thick black dashed line represents an empirically-fitted power law function, z^{-5}, for near-surface $<\varepsilon_L>$. The dotted blue line represents the z^{-3} fit for $<\varepsilon_S>$ and z is measurement depth to the water surface of the tank.